Electrochimica Acta 65 (2012) 127–133

Contents lists available at SciVerse ScienceDirect

Electrochimica Acta

journal homepage: www.elsevier.com/locate/electacta

Subfreezing operation of polymer electrolyte fuel cells: Ice formation and cell performance loss

Jeffrey Mishler[a], Yun Wang[a,*], Partha P. Mukherjee[b], Rangachary Mukundan[c], Rodney L. Borup[c]

[a] Renewable Energy Resources Lab (RERL), The University of California, Irvine, Irvine, CA 92697-3975, United States
[b] Texas A&M University, College Station, TX 77843, United States
[c] Los Alamos National Laboratory (LANL), Los Alamos, NM 87545, United States

ARTICLE INFO

Article history:
Received 10 November 2011
Received in revised form 6 January 2012
Accepted 7 January 2012
Available online 16 January 2012

Keywords:
Subfreezing operation
Polymer electrolyte fuel cells
Neutron imaging
Experiment
Modeling
Analysis

ABSTRACT

In this work, we investigate the cold-start operation of polymer electrolyte fuel cells (PEFCs) through high-resolution neutron radiography, experimental testing, theoretical evaluation, and comparison with model prediction. Ice formation location, voltage evolution, and loss of the electro-catalyst surface area (ECSA) are examined. A dimensionless parameter $\hbar$, characterizing the spatial variation of the reaction rate across the cathode catalyst layer, is discussed at subfreezing temperature using newly determined membrane ionic conductivity. The $\hbar$ evaluation identifies the operating range that the reaction rate can be treated uniform across the catalyst layer, in which the model is valid.

1. Introduction

The capability of polymer electrolyte fuel cells (PEFCs) to start up from subzero temperatures, also called cold start, is crucial to their transportation application. In subzero environments, water produced in electrodes freezes, resulting in reduced active electrochemical surface area and hindered reactant transport, see Fig. 1(a). The technical target set by the Department of Energy (DOE) for 2010 is the ability of the fuel cell stack to reach 50% rated power in 30 s starting from −20 °C, and the unassisted start-up temperature as low as −40 °C [1,2].

Cold-start experimental study has been attempted by several researchers [3–12]. Thompson et al. [7] used cryo-scanning electron microscopy to quantify the membrane water content, indicating that the membrane may absorb 14–15 water molecules per sulfonate group. Ge and Wang [8] presented a cyclic voltammetry (CV) study to investigate the effect of ice formation on the active catalyst area. Ishikawa et al. [9] investigated evidence of super-cooled water in the fuel cell, finding water freezing at the MEA/GDL interface. They expect that super-cooled water solidifies onto ice that remained after purging the fuel cell. Jiao et al. proposed different ice formation mechanisms for the cathode [10]. Jung and Um [11] investigated the effect of a vanadium oxide film over the bipolar plate on non-isothermal cold start performance, indicating that the added thermal resistance enables more reaction heat to heat up the fuel cell and prevent cold-start failure. Hou et al. studied sequential cold-start at different current densities and explored degradation in cold-start ability for sequential failed cold starts [12].

Cold-start models have been created by different research groups [13–20]. Wang [13] analyzed the key parameters such as the time constants and obtained solutions to voltage loss due to ice formation and further compared their effects. Mao et al. [14] presented a cold-start model accounting for heat and water transport as well as ice formation. Wang et al. [16] defined three cold-start stages and experimentally determined the ionic conductivity at subfreezing temperatures. Voltage variation during nonisothermal cold start was also analyzed. Meng [17,18] investigated the impact of several parameters on isothermal cold-start behaviors and indicated that high gas flow rate, low initial membrane water content, low current density, and high cell voltage are beneficial to fuel cell cold start. Balliet and Newman [19] presented a two-dimensional cold start model which was used to study cold start for ultrathin cathode catalyst layers. Jiang et al. [20] developed a three-dimensional multiphase model of non-isothermal cold start, where the water and heat transport is numerically treated using the generalized transport equation [21]. Their simulation indicated that lumped thermal analysis may overestimate the amount of heat required to ensure successful fuel cell start-up.

* Corresponding author. Tel.: +1 949 824 6004; fax: +1 949 824 8585.
E-mail address: yunw@uci.edu (Y. Wang).

0013-4686/$ – see front matter © 2012 Elsevier Ltd. All rights reserved.
doi:10.1016/j.electacta.2012.01.020

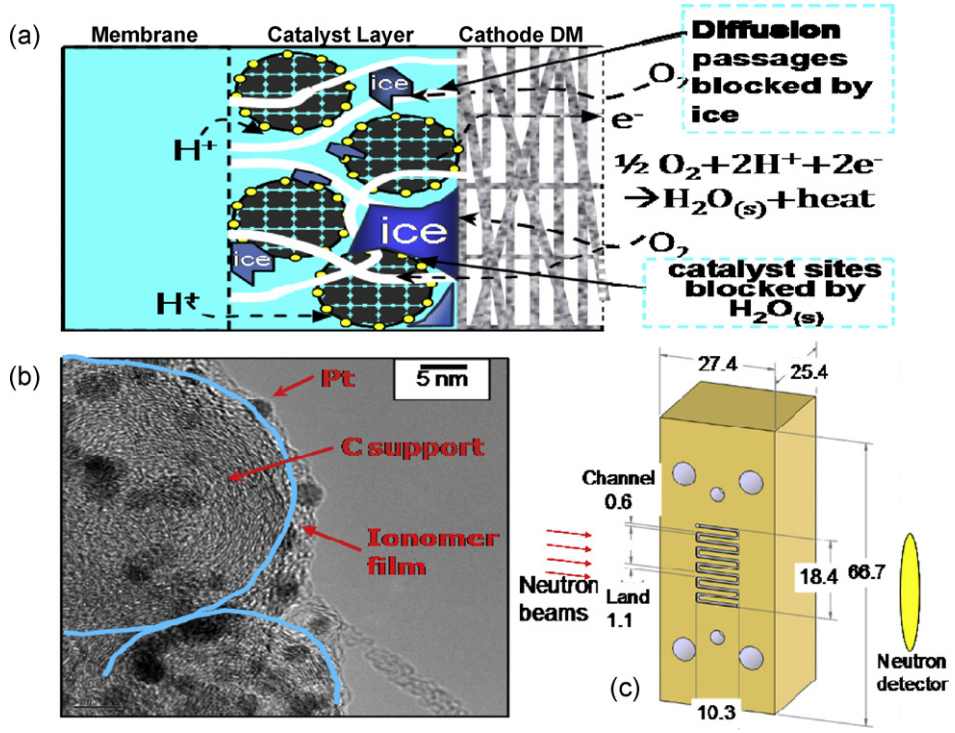

Fig. 1. Schematic of ice formation during fuel cell subfreezing operation (a); TEM of the catalyst layer surface (b); and the flow field design of the experimental PEFC for the neutron imaging studies (the unit: mm) (c).

Neutron imaging has been developed as a powerful tool for *in situ* measurements of the water content in fuel cells [22–28]. Owejan et al. [22,25] studied the water content in flow fields. Hickner et al. [26] measured the water distributions at operating conditions. Wang et al. [16] presented the water accumulations under channels and lands, respectively, for two subfreezing temperatures. Kramer and Zhang [27] investigated the liquid flow in flow fields and GDLs. Recently, a new detector technology based on micro-channel plates was installed at the NIST neutron facility [28], enabling higher resolution water detection.

Although a significant amount of effort has been made, several key aspects of cold start are still lacking and require further investigation. For example, most model predictions have not been validated yet. The location of ice formation is not fully understood and direct experimental visualizations are scarce. Few studies have addressed durability issues in freeze/thaw cycling. In this paper, several relevant aspects of fuel cell cold start are investigated. We first employ high-resolution neutron radiography to investigate ice location. Then the spatial variation of the reaction rate is discussed under subfreezing temperatures through evaluating a dimensionless parameter $\hbar$ using newly developed membrane ionic conductivity. By identifying the operating range that the reaction can be treated uniform across the catalyst layer in which the model is valid, we compared the model prediction with experimental data. Because of ice formation in the cathode and the high value the ice volume fraction can reach during cold start, cold start can affect catalyst layer durability. We also briefly examine the loss of the active catalyst surface area.

2. Experimental

Experiments were conducted on laboratory-scale fuel cells with a 50 cm^2 active area, and on neutron imaging-scale fuel cells with a 2.5 cm^2 active area. Various MEAs and GDLs were considered, as summarized in Table 1. The 50 cm^2 fuel cells had quad-serpentine flow fields, while the 2.5 cm^2 fuel cells had a single-serpentine flow field.

The fuel cells were first operated at 80 °C and a specified relative humidity (RH) at moderate current density, then shut down and purged with nitrogen at 2–5 L/min for 0.5–5 min. The temperature was then reduced to subzero using coolant flows. While at subzero temperature, the fuel cells were operated isothermally by applying a constant current at high stoichiometries until operation failure. Both high frequency resistance (HFR) and voltage evolution were measured. While operating under the above-described conditions, the 2.5 cm^2 fuel cells were imaged using the thermal beam line #2 neutron imaging facility at the NIST Center for Neutron Research (NCNR). Neutron radiographs were taken using the microchannel plate detector with a per-pixel spatial resolution of ~15 μm. The exposure time is 1 min. An example of neutron images is shown in Fig. 2(a) and (b), which clearly shows the MEA location, the middle bright region, because of ice production and accumulation. Fig. 2(c) presents the ice content profiles obtained through neutron imaging. The profiles were obtained by comparing dry and wet images

Table 1
MEAs and GDLs used in the experiment.

Components		Material configuration
MEA	Homemade ELAT decal-transfer MEA (0.2 mg/cm^2 Pt on Vulcan XC-72 carbon)	Nafion® 212 (50 μm, 0.2/0.2 mg Pt cm^{-2} anode/cathode
	Gore Primea	MESGA® (18 μm, 0.1/0.2 mg Pt cm^{-2} anode/cathode)
GDL	E-Tek ELAT cloth GDL	Double sided (cathode), single sided (anode)
	SGL low PTFE Paper GDL	24 B″C″ (5% PTFE in substrate and 5% PTFE in MPL)
	SGL high PTFE paper GDL	24 B″C″ (5% PTFE in substrate and 23% PTFE in MPL)

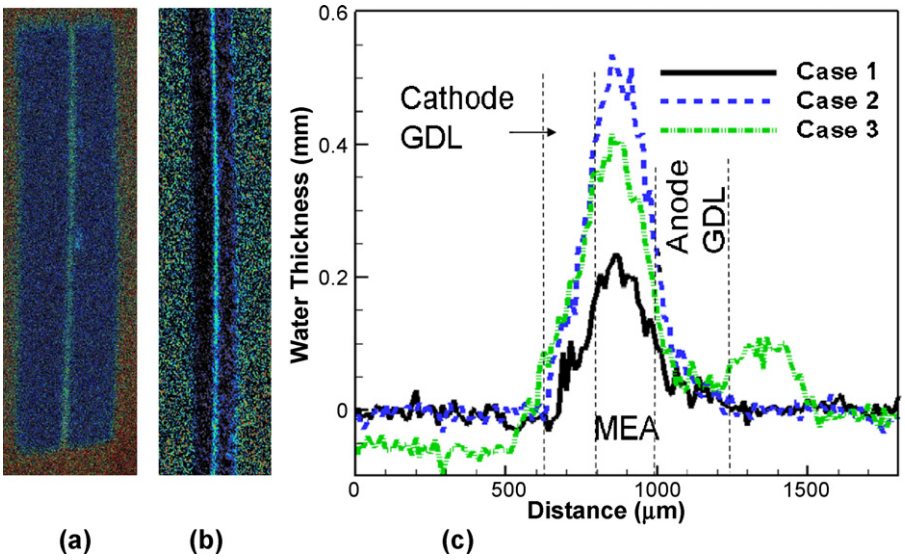

Fig. 2. Neutron images of water (ice) content in a fuel cell after cold start failure: (a) water content neutron image; (b) close-up image; and (c) water thickness in the PEFC detected by high-resolution neutron imagery. Cases 1, 2, and 3: cooling from 100, 50, and 50% relative humidities (RHs) and cold start at 0.04, 0.04, and 0.094 A/cm^2, respectively.

of the interested area which were taken when fuel cells shut down (before they produce water) and operate, respectively. It can be seen that the water thickness peaks appear in the cathode side of the MEA. It is worthy to note that the water content in the MEA and GDLs shown in the neutron images may be affected by experimental uncertainties such as geometrical blurs, which smooth the water content discontinuity occurring at the component interfaces [29]. However, the smoothing won't alter the local maximum in the water profile, *i.e.* the cathode side of the MEA has the highest ice thickness as indicated in the neutron images.

3. Theoretical analysis

As to the ice formed in the cathode catalyst layer, Wang [13] defined several stages in cold start: the first one is characterized by the water absorption process in the ionomer phase, bonding with the sulfonic acid groups; the second one starts with ice produced in the CL void space. Though the CL is thin (around 10 μm), the reaction can be highly non-uniform, which can be characterized by a dimensionless parameter $\hbar$ [30]:

$$\hbar = \frac{|j_0 - j_\delta|}{\int_0^1 j(\bar{x})d\bar{x}} = \frac{|j_0 - j_\delta|}{I/\delta_{CL}} \tag{1}$$

where j is the transfer current density, and j_0 and j_δ are the transfer current densities at the two surfaces of the catalyst layer, respectively. $\bar{x}$ is the dimensionless distance in the through-plane direction and δ the thickness. Through rigorous derivation of the local reaction rate profile, one can reach [30]:

$$\hbar = \frac{\Delta U}{2(R_g T/\alpha_c F)} \text{ where } \Delta U = \frac{I\delta}{\sigma_m^{\text{eff}}} = IR_\delta \tag{2}$$

Under small $\hbar$s (*e.g.* low currents), the reaction can be treated uniform, therefore the reaction water is uniformly added to the CL. However, it must be carefully examined at subfreezing operation because of the effects of temperature and freezing water in Nafion membranes on their ionic conductivity. Fig. 3 plots $\hbar$ as a function of temperature and ΔU for several operating temperatures, indicating small difference among the temperatures. It can be seen that the reaction is almost uniform for $\Delta U < 0.05$ V. Note that ΔU is a function of temperature when using Nafion as the electrolyte. One of the most prevalently used proton-conductivity models is the empirical correlation developed by Springer et al. [31] for the Nafion® 117 membrane, which was based on experimental data measured at 30 °C. Our recent measurement indicated that the ionic conductivity at subfreezing temperature is lower than that of Springer et al. in some regions, see Fig. 4:

$$\begin{aligned}\sigma_m &= (0.01862\lambda - 0.02854)\exp\left[4029\left(\frac{1}{303} - \frac{1}{T}\right)\right] \text{ or} \\ &= (0.004320\lambda - 0.006620)\exp\left[4029\left(\frac{1}{273} - \frac{1}{T}\right)\right] \\ &= \sigma_{m,0}(\lambda)\exp\left[4029\left(\frac{1}{273} - \frac{1}{T}\right)\right] \quad \text{for} \quad \lambda \le 7.22 \\ \sigma_m &= \sigma_m(\lambda = 7.22) \quad \text{for} \quad \lambda > 7.22\end{aligned} \tag{3}$$

Fig. 5 compares ΔUs at different current densities using the two ionic conductivity correlations (at $\lambda = 14$). It can be seen that that at the lowest currents both correlations result in a small $\Delta U < 0.02$ V at −30 °C, while at 0.1 A/cm^2 ΔU is over 0.1 V at −30 °C using

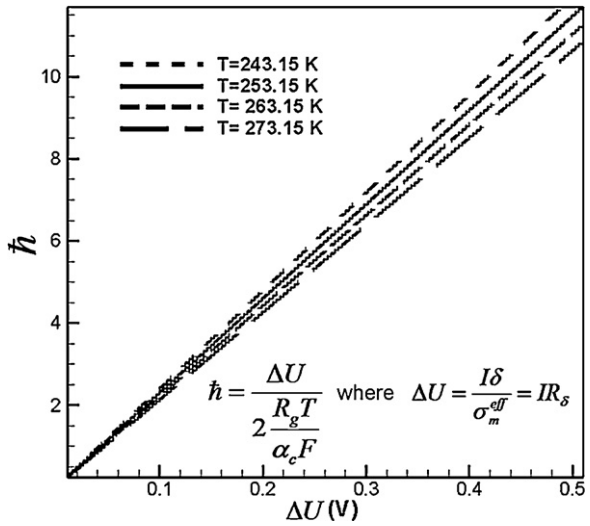

Fig. 3. The value of $\hbar$ as a function of temperature and ΔU for several typical operating temperatures.

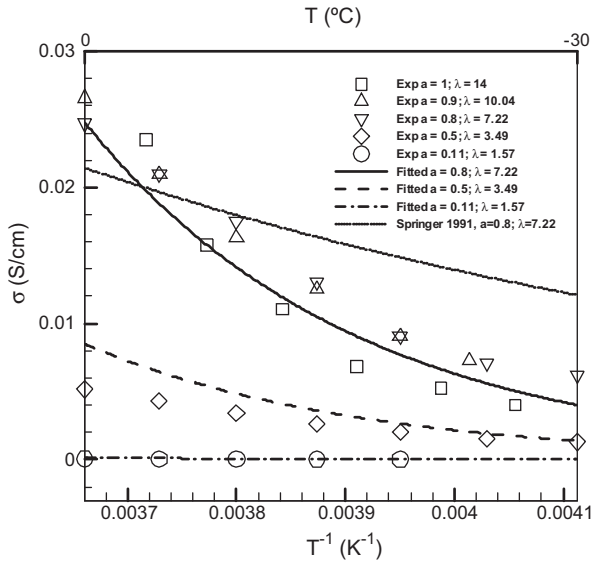

Fig. 4. The dependence of the ionic conductivity on temperature and water content based on Nafion®.

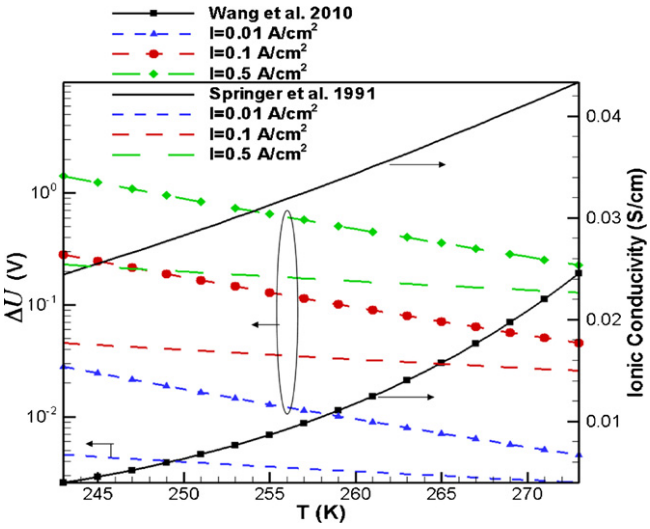

Fig. 5. The value of ΔU as a function of temperature and current density.

the correlation of Wang et al. [16]. Note that ΔU of 0.1 V yields $\hbar$ over 2 or a considerable variation in the reaction rate; however, using that of Springer et al. [31] results in a small value of ΔU (<0.03 V) at −30 °C at this current. For 0.5 A/cm^2, ΔU is even over 1 at −30 °C. Thus, for currents around 0.01 A/cm^2 or lower we can assume uniform water production across the cathode catalyst layer during fuel cell cold start. For the case of the present experiment where the temperature was set at −10 °C, both ΔUs are around 0.008 V at 0.01 A/cm^2, which yield a very small $\hbar$ (<0.2). However, at 0.1 A/cm^2 and −10 °C, the correlation of Wang et al. indicates a ΔU of around 0.08 V in which $\hbar$ is around 2.

4. A cold-start model

It is likely true that only the solid water in the cathode CL has a significant impact on the electrochemical reaction. One reason is that the ice holding capability of the GDLs is much larger than of the CL. In addition, at the low current densities frequently encountered in cold start, the oxygen concentration drop across a GDL is negligibly small. Focusing on the cathode CL, the net water addition can be formulated using the net water transfer coefficient α. To make it general, we can assume α also takes into accounts for the water transport into GDLs. A mathematical cold-start model was proposed by Wang [13] to predict the voltage loss and ice volume fraction. The model assumes that the reaction rate is uniform in the cathode catalyst layer, which is valid in the current density of 0.02 A/cm^2 in the experiment as indicated by the previous $\hbar$ evaluation. Model detail refers to Ref. [13] and is not repeated here. The ice volume fraction in void is obtained through comparing the net water addition rate and entire pore space:

$$s_{\text{ice}}(t) = \frac{V_{\text{ice}}}{V_{\text{pore}}} = \frac{t}{\tau_{\text{ice},2}} - k_\tau \quad \text{where } \tau_{\text{ice},1} = \frac{2F\rho_m\varepsilon_m\delta_{CL}(14-\lambda_0)}{(1+2\alpha)EW*I},$$

$$\tau_{\text{ice},2} = \frac{2F\rho_{\text{ice}}\varepsilon_{CL}\delta_{CL}}{(1+2\alpha)M^wI}, \quad k_\tau = \frac{\rho_m\varepsilon_m(14-\lambda_0)M^w}{\rho_{\text{ice}}\varepsilon_{CL}EW} \tag{4}$$

Ice presence can affect the electrode electrochemical activity and hence the cell voltage loss. The effect can be formulated by using the modified Butler–Volmer equation:

$$j = -a_0 i_{0,c}^{\text{ref}}(1-s_{\text{ice}})^{\tau_a}\exp\left[-\frac{E_a}{R}\left(\frac{1}{T}-\frac{1}{353.15}\right)\right] \times \frac{C^{O_2}}{C^{O_2,\text{ref}}}\exp\left(-\frac{\alpha_c F}{RT}\cdot\eta\right) \tag{5}$$

Because of the uniformity of the reaction rate at 0.02 A/cm^2, the local transfer current can be calculated by:

$$j = -\frac{I}{\delta_{CL}} \tag{6}$$

The voltage loss is governed by several major mechanisms, and can be expressed as:

$$V_{\text{cell}} = U_o + \eta_c - \eta_a - R_\Omega I \tag{7}$$

The last term on the right side represents the voltage loss due to the ohmic resistance. The cathode overpotential η_c contributes a considerable portion of voltage loss, primarily due to the sluggish ORR (oxygen reduction reaction). Solid water influences the voltage loss in two primary ways [13]: one is to narrow the oxygen transport passage; the other is covering and hence reducing the electro-catalyst surface area (ECSA). By substituting the volume fraction of ice from Eq. (4) into Eq. (5) and utilizing the oxygen profile obtained in Ref. [13], one can decouple the cathode overpotential:

$$\eta_c(s_{\text{ice}}, T, \bar{x}) = \eta_{c,0} + \Delta\eta_{c,T} + \Delta\eta_{C,1} + \Delta\eta_{C,2} \tag{8}$$

where

$$\eta_{c,0} = -\frac{R_gT}{\alpha_cF}\ln\left(\frac{IC^{O_2,\text{ref}}}{a_o i_{0,c}^{\text{ref}}\ \exp[-(E_a/R_g)((1/T_0)-(1/353.15))]C_{cCL}^{O_2}\delta_{CL}}\right),$$

$$\Delta\eta_{c,T} = -\frac{TE_a}{\alpha_cF}\left(\frac{1}{T}-\frac{1}{T_o}\right), \quad \Delta\eta_{C,1} = \frac{R_gT\tau_a}{\alpha_cF}\ln(1-s_{\text{ice}}) \quad \text{and} \quad \Delta\eta_{C,2} = \frac{R_gT}{\alpha_cF}\ln\left(1-Da\frac{1-\bar{x}^2}{\varepsilon_{CL}^{\tau_d-\tau_{d,0}}(1-s_{\text{ice}})^{\tau_d}}\right)$$

where $\bar{x}$ is the dimensionless distance, $\Delta\eta_{C,1}$ the voltage loss caused by the increased transport resistance due to solid water presence, $\Delta\eta_{C,2}$ the loss associated with the reduced ECSA, and Da the

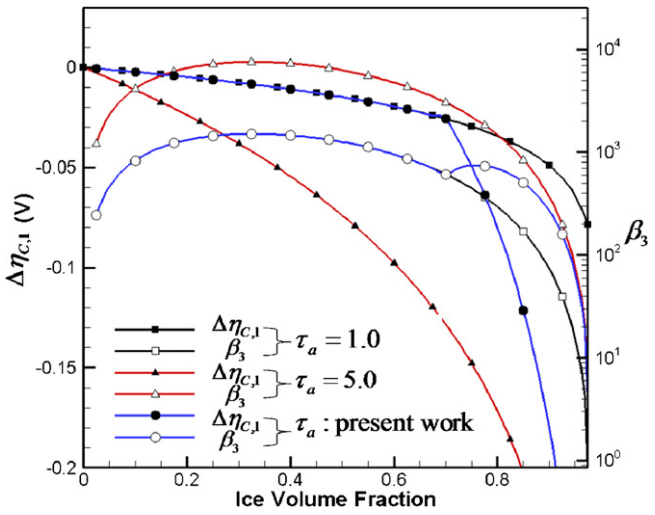

Fig. 6. The values of $\Delta\eta_{c,1}$ and β_3 as a function of τ_a and ice volume fraction at $\tau_d = 2.5$.

Damköhler number [13]. Physically, $\eta_{c,0}$ denotes the overpotential at the interface between the cathode CL and GDL when no ice is present. Two important factors affect the voltage loss, they are τ_a and τ_d. Ref. [13] discussed detail about the influence of τ_d, and also defined a parameter β_3 to the two effects of ice:

$$\beta_3 = \frac{\Delta\eta_{c,1}}{\Delta\eta_{c,2}} \tag{9}$$

Fig. 6 displays the effects of τ_a on $\Delta\eta_{C,1}$ at $\tau_d = 2.5$, along with β_3. It can be seen that the value of β_3 increases at first and drops when the ice volume fraction is close to 1. In most regions, the magnitude of $\Delta\eta_{C,1}$ is much higher than that of $\Delta\eta_{C,2}$.

5. Results and discussion

Fig. 7(a) shows the voltage evolution in the subfreezing operation at −10 °C. Both cases indicate negligible negative impacts of solid water on cell performance at the initial stage; the fast voltage drop occurs near the operation shut down. In the model validation, we found that the factor of the ice coverage τ_a may not be a constant, instead depends on the ice content and can be a large value. To best match the experimental data, we used a constant τ_a of 1.0 in the range of $s_{ice} < 0.7$, then a linear increased to 5 from $s_{ice} = 0.7$ to 0.1, see Fig. 7(d). The possible explanation to adopting the varying τ_a is that at a low content ice may exist as small isolated islands over the thin ionomer film surface, allowing adequate oxygen access to catalyst through the lateral direction, see Fig. 7(b). As solid water accumulates, the isolated islands merge, forming a thin but long stretched thin layer. The layer can effectively disable oxygen transport toward the catalyst, shutting down local catalyst activity. Note that a thin layer of solid water can significantly disable the local catalyst reactivity, see Fig. 7(c). For the tortuosity of the pore space, we chose $\tau_d = 2.5$. Fig. 6 displays $\Delta\eta_{C,1}$, along with β_3 for the adopted profile of τ_a, indicating that the value of τ_a around 5 results in a considerable effect on voltage loss.

Table 2
ECSA Loss after cold-start cycling.

Cell description	ECSA loss after 4 starts	ECSA loss after 10 or 11 cycles
Gore MEA/low PTFE paper GDL	46%	53% (11 starts)
Gore MEA/high PTFE paper GDL	21%	32% (10 starts)

The ECSA is an important factor characterizing the electrode performance. The surface is usually referred to as the triple-phase boundaries (TPB) of the ionomer, carbon-supported catalyst, and gas phase. This reaction surface can be permanently damaged during freeze/thaw cycling. One reason is due to the solid–liquid phase change, which may deform and permanently damage the CL microstructure. Note that Wang [13] indicated that the time constant of ice melting is short <1 s. Further, most ice exists in the cathode CL, see Fig. 2, and ice may occupy nearly the entire void space in the cathode CL during cold start [13]. Another cause of degradation can be the oxygen starvation due to ice presence, which may lead to loss of the carbon support. To quantify the ECSA loss, we conducted cyclic voltammetry (CV) testing before and after cold start. The CV technique has been frequently used to evaluate the ECSA of Pt/C catalysts by adsorption of atomic hydrogen in acidic media [32]. Fig. 8 shows the curves of the voltage and current at a voltage sweeping rate of 60 mV/s. Table 2 summaries the ECSA loss after 4 starts and around 10 at −10 °C. It can be seen that the ECSA loss is severe after the first four cycles: for the high PTFE loading case, 46% reduction is indicated after the

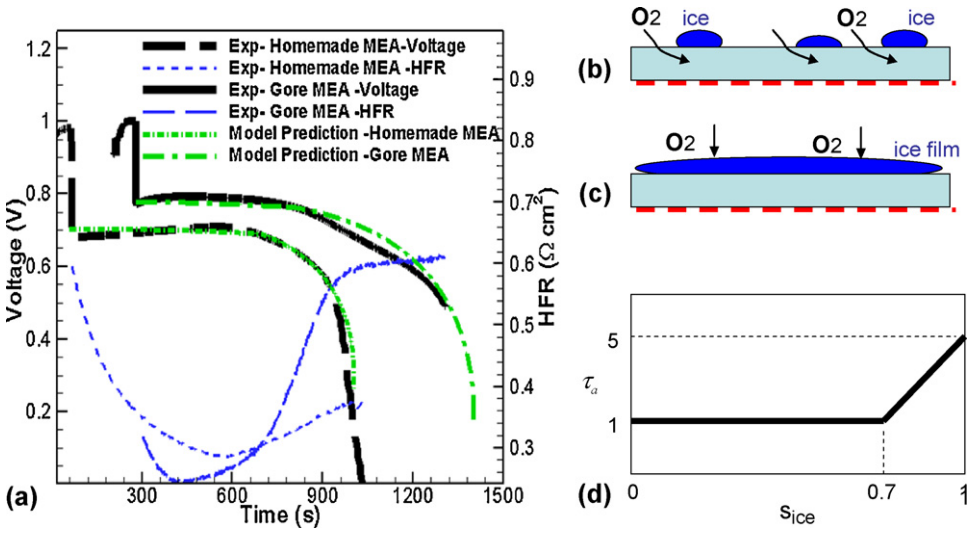

Fig. 7. (a) Transient response of cell voltages and HFR (high frequency resistance) during subfreezing operations at 0.02 A/cm^2 and −10 °C; (b) solid water islands scatter over the thin ionomer film, allowing oxygen access to the catalyst (dashed line); (c) ice islands connect, forming thin ice layer and blocking oxygen access to local catalyst; and (d) the factor of the ice coverage τ_a used in the model validation.

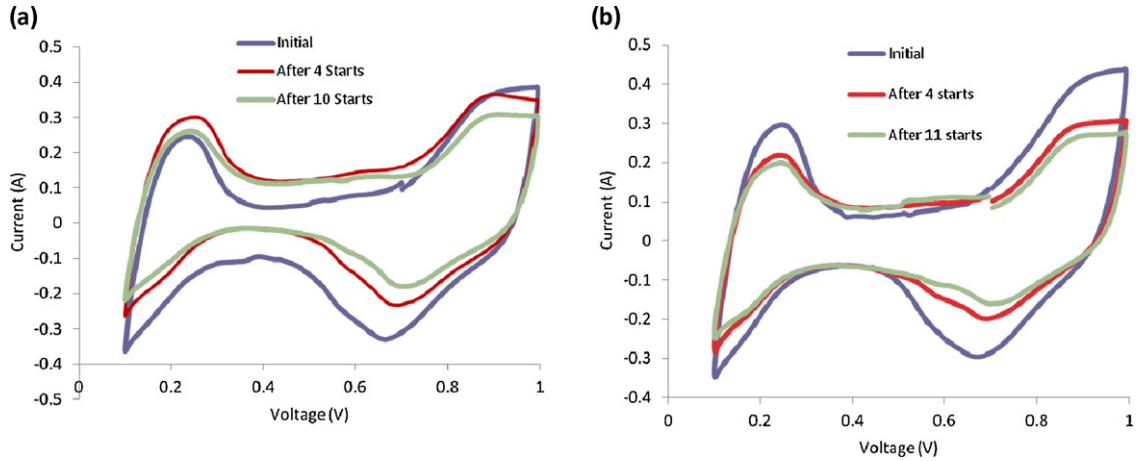

Fig. 8. The CV testing at the sweeping rate of 60 mV/s for fuel cells with (a) high-PTFE carbon paper and (b) low-PTFE carbon paper. The corresponding ECSA losses are listed in Table 2.

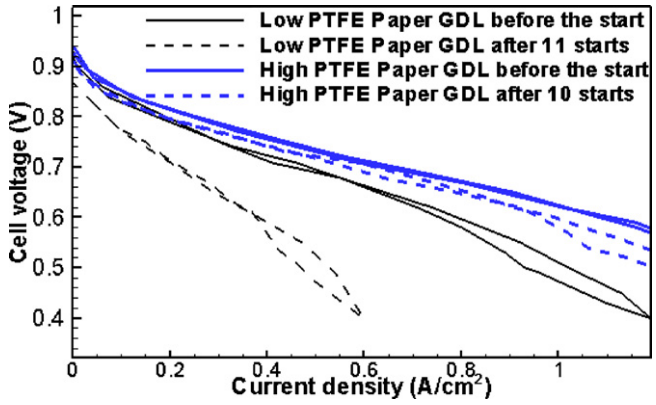

Fig. 9. Fuel cell performance before/after cold starts for Gore MEAs at −10 °C. Table 2 lists the values of the ECSA loss.

first four cycles, and 53% after the eleven cycles. The other case also shows the same trend. The table also indicates that the higher the PTFE loading the smaller the ECSA loss for the fuel cells. This may be explained by the liquid water drainage during ice melting: the higher loading improves liquid water removal. Fig. 9 displays the cell performances before and after 10–11 cold starts at normal temperature, clearly indicating cell performance decays and confirming the ECSA loss calculated by the CV technique. Again, the higher PTFE loading yields a smaller performance decrease due to the less ECSA loss.

6. Conclusions

In this study, we first conducted high-resolution neutron radiography to probe ice formation in PEFCs and found that the peak of ice thickness exists in the cathode side of the MEAs. The nonuniformity parameter $\hbar$ was evaluated at subfreezing temperature, indicating that the reaction is almost uniform across the catalyst layer around 0.01 A/cm^2 or lower even at −30 °C. Using newly measured ionic conductivity of membrane at subfreezing temperature, the $\hbar$ evaluation showed that a considerable variation of reaction rate across the catalyst layer may occur even around 0.1 A/cm^2. We also found that ice formation significantly affects the electrochemical activity in the later operation stage before the voltage drops to zero. By assuming the varying coefficient of ice coverage effect on the ECSA, we compared the model prediction with experimental results, showing a good agreement. The cold-start cycling testing indicated the ECSA loss and consequent cell performance decrease occurred after four and about ten cycles. The ECSA loss is severe in the first four cycles, and the PTFE loading can affect the ECSA and performance loss. The corroboration of modeling prediction with the experimental transient voltage response and the $\hbar$ evaluation are key highlights.

Appendix A. Nomenclature

a	effective catalyst area per unit volume, m^2/m^3
a_o	catalyst surface area per unit volume, m^2/m^3
C	molar concentration of species k, mol/m^3
D	species diffusivity, m^2/s
EW	equivalent weight of dry membrane, kg/mol
F	Faraday's constant, 96,487 C/equivalent
I	current density, A/cm^2
i	superficial current density, A/cm^2
j	transfer current density, A/cm^3
M	molecular weight, kg/mol
P	pressure, Pa
R	universal gas constant, 8.134 J/mol K; ohmic resistance, mΩ cm^2
s_{ice}	ice volume fraction
t	time, s
T	temperature, K
U_o	equilibrium potential, V

Greek letters

α	transfer coefficient; net water flux per proton flux
ρ	density, kg/m^3
ϕ	phase potential, V
σ	ionic conductivity, S/m
λ	membrane water content, # of H_2O/SO_3H-group
ε	porosity
η	surface overpotential, V
τ	tortuosity/coverage coefficient; time constant, s
δ	thickness, m

Superscripts and subscripts

c	cathode
CL	catalyst layer
d	diffusion
e	electrolyte

eff	effective value
g	gas phase
m	membrane phase
o	reference value; initial value
ref	reference value
w	water

References

[1] EERE, Hydrogen, Fuel Cells & Infrastructure Technologies Program Multi-Year Research, Development and Demonstration Plan, 2007, p. 14.
[2] Y. Wang, K. Chen, J. Mishler, S.C. Cho, X. Cordobes Adroher, Applied Energy 88 (4) (2011) 981.
[3] Y. Hishinuma, T. Chikahisa, F. Kagami, T. Ogawa, JSME International Journal Series B Fluids and Thermal Engineering 47 (2) (2004) 235.
[4] R.C. McDonald, C.K. Mittelsteadt, E.L. Thompson, Fuel Cells 4 (3) (2004) 208.
[5] E. Cho, J.J. Ko, H.Y. Ha, S.A. Hong, K.Y. Lee, T.W. Lim, I.H. Oh, Journal of the Electrochemical Society 151 (5) (2004) A661.
[6] M. Oszcipok, D. Riemann, U. Kronenwett, M. Kreideweis, M. Zedda, Journal of Power Sources 145 (2) (2005) 407.
[7] E.L. Thompson, J. Jorne, W.B. Gu, H.A. Gasteiger, Journal of the Electrochemical Society 155 (6) (2008) B625.
[8] S. Ge, C.-Y. Wang, Journal of the Electrochemical Society 154 (12) (2007) B1399.
[9] Y. Ishikawa, et al., Super-cooled water behavior inside polymer electrolyte fuel cell cross-section below freezing temperature, Journal of Power Sources 179 (2) (2008) 547.
[10] K. Jiao, et al., Cold start characteristics of proton exchange membrane fuel cells, International Journal of Hydrogen Energy 36 (18) (2011) 11832.
[11] H.-M. Jung, S. Um, An experimental feasibility study of vanadium oxide films on metallic bipolar plates for the cold start enhancement of fuel cell vehicles, International Journal of Hydrogen Energy 36 (24) (2011) 15826.
[12] J. Hou, et al., Reversible performance loss induced by sequential failed cold start of PEM fuel cells, International Journal of Hydrogen Energy 36 (19) (2011) 12444.
[13] Y. Wang, Journal of the Electrochemical Society 154 (10) (2007) B1041.
[14] L. Mao, C.-Y. Wang, Y. Tabuchi, Journal of the Electrochemical Society 154 (3) (2007) B341.
[15] K. Jiao, X. Li, Three-dimensional multiphase modeling of cold start processes in polymer electrolyte membrane fuel cells, Electrochimica Acta 54 (27) (2009) 6876.
[16] Y. Wang, P.P. Mukherjee, J. Mishler, R. Mukundan, R.L. Borup, Electrochimica Acta 55 (8) (2010) 2636.
[17] H. Meng, Numerical studies of cold-start phenomenon in PEM fuel cells, Electrochimica Acta 53 (22) (2008) 6521.
[18] H. Meng, B. Ruan, Numerical studies of cold-start phenomena in PEM fuel cells: A review, International Journal of Energy Research 35 (1) (2011) 2.
[19] R.J. Balliet, J. Newman, Cold-start modeling of a polymer-electrolyte fuel cell containing an ultrathin cathode, Journal of the Electrochemical Society 158 (9) (2011) B1142.
[20] F. Jiang, W. Fang, C.-Y. Wang, Non-isothermal cold start of polymer electrolyte fuel cells, Electrochimica Acta 53 (2) (2007) 610.
[21] C.-Y. Wang, Fundamental models for fuel cell engineering, Chemical Reviews 104 (10) (2004) 4727.
[22] A.B. Geiger, A. Tsukada, E. Lehmann, P. Vontobel, A. Wokaun, G.G. Scherer, Fuel Cells 2 (2) (2002) 92.
[23] K.L. Moore, K.S. Reeves, DOE Hydrogen Program Annual Merit Review Proceedings, Arlington, VA, USA, May 23–26, 2005.
[24] T.A. Trabold, J.P. Owejana, D.L. Jacobson, M. Arif, P.R. Huffman, International Journal of Heat and Mass Transfer 49 (25–26) (2006) 4712.
[25] J.P. Owejan, T.A. Trabold, D.L. Jacobson, D.R. Baker, D.S. Hussey, M. Arif, International Journal of Heat and Mass Transfer 49 (25–26) (2006) 4721.
[26] M.A. Hickner, N.P. Siegel, K.S. Chen, D.S. Hussey, D.L. Jacobson, M. Arif, Journal of the Electrochemical Society 155 (3) (2008) B294.
[27] D. Kramer, J. Zhang, Electrochimica Acta 50 (13) (2005) 2603.
[28] D.S. Hussey, D.L. Jacobson, M. Arif, J.P. Owejan, J.J. Gagliardo, T.A. Trabold, Journal of Power Sources 172 (1) (2007) 225.
[29] Y. Wang, K.S. Chen, Journal of the Electrochemical Society 157 (12) (2010) B1878.
[30] Y. Wang, X. Feng, Journal of the Electrochemical Society 155 (12) (2008) B1289.
[31] T.E. Springer, T.A. Zawodinski, S. Gottesfeld, Journal of the Electrochemical Society 126 (1991) 2334.
[32] A. Pozio, M. De Francesco, A. Cemmi, F. Cardellini, L. Giorgi, Comparison of high surface Pt/C catalysts by cyclic voltammetry, Journal of Power Sources 105 (1) (2002) 13.